Real-Time X-ray Absorption Spectroscopy of Uranium, Iron, and Manganese in Contaminated Sediments During Bioreduction

Tetsu K. Tokunaga[*1], Jiamin Wan[1], Yongman Kim[1], Steve R. Sutton[2], Matthew Newville[2], Antonio Lanzirotti[2], and William Rao[3]

[*]Corresponding author phone (510) 486-7176; e-mail: tktokunaga@lbl.gov

[1]Lawrence Berkeley National Laboratory, Berkeley, California 94720

[2]University of Chicago, Chicago, Illinois 60637

[3]Savannah River Ecology Laboratory, University of Georgia, Aiken, South Carolina 29802

Abstract

The oxidation status of uranium in sediments is important because the solubility of this toxic and radioactive element is much greater for U(VI) than for U(IV) species. Thus, redox manipulation to promote precipitation of UO_2 is receiving interest as a method to remediate U-contaminated sediments. Presence of Fe and Mn oxides in sediments at much higher concentrations than U requires understanding of their redox status as well. This study was conducted to determine changes in oxidation states of U, Fe, and Mn in U-contaminated sediments from Oak Ridge National Laboratory. Oxidation states of these elements were measured in real-time and nondestructively using X-ray absorption spectroscopy, on sediment columns supplied with synthetic groundwater containing organic carbon (OC, 0, 3, 10, 30 and 100 mM OC as lactate) for over 400 days. In sediments supplied with OC $\geq$ 30 mM, 80% of the U was reduced to U(IV), with transient reoxidation at about 150 days. Mn(III,IV) oxides were completely reduced to Mn(II) in sediments infused with OC $\geq$ 3 mM. However, Fe remained largely unreduced in all

sediment columns, showing that Fe(III) can persist as an electron acceptor in reducing sediments over long times. This result in combination with the complete reduction of all other potential electron acceptors supports the hypothesis that the reactive Fe(III) fraction was responsible for reoxidizing U(IV).

Introduction

The mobility of U through sediments is strongly influenced by its oxidation state (*1*). Reduction of U(VI) to less soluble U(IV) occurs through metal (primarily Fe) and sulfate reducing microorganisms (2-4), and through abiotic redox reactions with Fe(II) (5), green rusts (6), and S(-II) (7). Conversely, oxidation of U(IV) to U(VI) occurs rapidly in the presence of oxygen (*8, 9*), nitrate/nitrite (*10, 11*), Mn(III,IV) (12), and some Fe(III) (hydr)oxides (13-16). The behavior of U in sediments during the transition from oxidizing to reducing conditions is complicated because of coupling between numerous reactions, with transformations progressing at widely varying rates.

In our previous study on historically U-contaminated Oak Ridge National Laboratory sediments, U(IV) reoxidation occurred under sustained reducing conditions (*14, 17*). Uranium-contaminated sediments were infused with a steady supply of organic carbon (OC, 10.7 mM lactate = 32 mM OC, at an OC supply rate of 0.55 mmol kg^{-1} d^{-1}). Changes in U oxidation states were determined nondestructively within columns using micro- X-ray absorption near edge structure (µ-XANES) spectroscopy. Rapid U(VI) reduction during the initial 80 days was followed by reoxidation of U(IV) and increased U(VI) concentrations in effluents. Reoxidation of U(IV) was unexpected because these columns were maintained under continuously reducing conditions. We found that U(VI) enrichment in effluents resulted from complexation with

carbonates produced by microbial OC oxidation. Reactive Fe(III) and/or Mn(IV) oxides were suspected as the terminal electron acceptors (TEAs) for U(IV) reoxidation, but that earlier experimental system did not permit direct, nondestructive speciation of Fe and Mn.

This present study follows the course of the previous work, with the main goal of testing the hypothesis that Fe(III) and Mn(III,IV) oxides persist long enough during U bioreduction to permit U reoxidation under sustained metal-reducing conditions. The experiments involved infusion of synthetic groundwater containing different concentrations of OC into U-contaminated sediments, and periodically obtaining µ-XANES spectra of U, Mn, and Fe to directly monitor oxidation states of each element. In this paper, OC does not refer to native sediment organic matter unless indicated. The study presented here is part of a larger effort designed to understand impacts of different OC forms and supply rates on U transformations and on microbial communities.

Materials and Methods

Sediment. Uranium-contaminated sediment was obtained from the U.S. Department of Energy's Environmental Remediation Science Program's Field Research Center (FRC) at Oak Ridge National Laboratory. The sediment had a total U concentration of 1.08 mmol kg^{-1} (X-ray fluorescence analysis, XRF), and was from a location near that of our previous study (14). The total Mn and Fe in this sediment were 49.1 and 1,185 mmol kg^{-1}, respectively (XRF). Citrate-dithionite method (*18*) yielded an extractible Fe concentration of 248 mmol kg^{-1}. A 0.5 M HCl extraction paired with a 0.25 M HCl/hydroxylamine hydrochloride extraction (*19*) yielded an extractible Fe(II) concentration of 0.23 mmol kg^{-1}, and operationally defined microbially reducible Fe(III) concentration of 5.9 mmol kg^{-1}. This sediment had a native OC concentration of

370 mmol kg^{-1} (0.44%). Additional geochemical analyses of the sediment are provided in Supporting Information Table S1. Moist sediment was passed through a 4.75 mm sieve and homogenized prior to packing into columns to a porosity of 0.51.

Sediment columns. 200 mm long, 31.5 mm inner diameter polycarbonate columns were similar to those used previously (14), except that thinner windows were installed to permit sufficient X-ray penetration into sediments and fluorescent X-ray collection at the lower energies of Mn and Fe K absorption edges. In order to maintain the structural integrity of each column, the windows were made in 2 sections (70 mm by 10 mm) separated by a solid pipe segment (Supporting Information, Figure S1). Two layers of Kapton tape were use for each window, such that the adhesive surfaces were sandwiched between Kapton films in order to prevent redox reactions between the sediment and adhesive (*20*). Kapton windows were secured on columns with aluminum frames (0.60 mm thick), and caulked with epoxy glue. Windows were covered with plastic plates banded to the column in order to limit slow expansion of the sediment against the thin Kapton film, and uncovered during µ-XANES data collection. Platinum redox electrodes were embedded into each column at distances of 50, 100, and 150 mm.

Influent solutions. A synthetic groundwater solution was prepared based on the composition of an uncontaminated groundwater from the Oak Ridge FRC. Its major ion chemistry consisted of 0.83 mM Ca^{2+}, 0.20 mM Mg^{2+}, 2.00 mM Na^{+}, 0.10 mM K^{+}, 2.1 mM Cl^{-}, 1.00 mM HCO_3^{-}, 0.50 mM SO_4^{2-}, and 0.05 mM NO_3^{-}, had an ionic strength of 5.68 mM, pCO_2 ≈3.5, and pH = 7.3. Low levels of NO_3^{-} and SO_4^{2-} were included in these solutions because of their natural occurrence in groundwater, hence their likely inclusion in remediation relying on injection of OC-amended local groundwater. For the OC supply at different concentrations, Na-lactate was

added to the synthetic groundwater to obtain solutions containing 0, 3, 10, 30, and 100 mM OC, with all solutions autoclaved.

Sediment column operation. Columns were kept in an N_2-purged glovebox except during times for transporting to synchrotron facilities for µ-XANES data collection. Solutions were supplied via syringe pumps at an average pore water velocity of 8.2 mm day^{-1} (24 day residence time). After supplying columns with 2 pore volumes (1 PV = 79.5 mL) of the 0 mM OC solution, infusion with different OC concentration solutions (including continuation of one column with 0 mM OC) was initiated. The combination of influent OC concentrations and pump rate yielded column-averaged supply rates ranging from 0 to 1.4 mmol OC kg^{-1} day^{-1}. Effluents were collected using a fraction collector. Redox potentials were periodically obtained by Pt electrode readings referenced to a calomel electrode tapped into the outflow end of each column. When columns were to be transported to synchrotron facilities, endcap valves were shut and disconnected from inflow/outflow lines, and columns were sealed in individual N_2-purged plastic bags.

Micro-XANES spectroscopy. Oxidation states of U, Fe, and Mn in sediments were obtained using µ-XANES spectroscopy (*21, 22*). The X-ray absorption spectra of each of these elements were obtained at the GeoSoilEnviroCARS beamline 13ID-C at the Advanced Photon Source (APS, Argonne National Laboratory, Argonne, IL), and at beamline X26A of the National Synchrotron Light Source (NSLS, Brookhaven National Laboratory, Upton, NY). At both facilities, beam sizes of ≈200 µm (vertical) by ≈800 µm (horizontal) were used in order to average over a large population of mineral grains and pores. The broad beam size also helped minimize X-ray beam-induced reduction (*23*). Profiles of µ-XANES spectra were obtained

along each sediment column, sequentially for Mn, Fe and U, at 7 different times during the course of this study.

Oxidation state standards for Mn consisted of $MnCO_3$ for defining the Mn(II) edge energy, Na-birnessite, MnO_2 for defining the Mn(IV) edge energy, and $KMnO_4$ for energy calibration, each mixed into SiO_2 powder to about 1% Mn. A Mn(III) standard was not included because of the priority placed on determining redox status within the range set by Mn(IV) and Mn(II), and the interest in avoiding radiation-induce redox changes. Resolution of all 3 Mn oxidation states would require longer X-ray exposures for collection of µ-XANES data at high resolution. The Mn(VII) pre-edge peak energy was set equal to 6,543.3 eV (*24*). Examples of these Mn K-edge spectra are shown in Figure 1a. Because several different energy steps were taken within individual scans, spectra were smoothed piecewise using an extension of the Savitzky-Golay method developed by Gorry (*25*). This smoothing was also applied to the Fe and U spectra. Manganese K-edge scans on soils were obtained with coarse steps in the below edge region (6,530 to 6540 eV, in 2 eV step), finer steps in the edge region (6541 to 6565 eV, in 0.5 eV steps), and coarse steps above the absorption edge (6,630 to 6,650 eV, in 5 eV steps) for normalizing the step height. The Mn µ-XANES measurements on sediment columns were done with high resolution only along the main absorption edge in order to minimize the potential for X-ray beam induced redox changes. Local Mn redox status was characterized by determining the energy along the absorption edge corresponding to half the absorption of the step height (*26*), then comparing this half-height energy to those of Mn(II) and Mn(IV) standards. These edge energies differ by 6.0 ±0.5 eV.

Iron oxidation states were characterized using the energy of the 1s-3d pre-edge centroid, which shifts about -2.5 eV in going from Fe(III) to Fe(II) (*27-29*). Oxidation state standards

used were hematite and goethite for Fe(III), and fayalite for Fe(II), with their spectra shown in Figure 1b. An Fe foil was used for energy calibration, with its edge energy taken as 7,112.0 eV. With this calibration, the pre-edge centroid energies for hematite and goethite standards were 7,114.9 ±0.1 eV. Distinguishing among different Fe(III) oxides within sediments by XANES spectroscopy is challenging (*30*), and was not attempted. Iron K-edge spectra were collected over energy ranges starting at or below 7,050 eV and finishing at 7,300 eV or higher, with 0.1 eV steps in the pre-edge region (7,110 to 7,120 eV), and coarser (0.25 to 2 eV) steps elsewhere.

Oxidation states for U in sediments were obtained through determining U L_{III} absorption edges, specifically through the edge energies at half that of the step height (*31*). Monochromatic X-ray energies were scanned from about -40 to +200 eV relative to the U L_{III} absorption edge, using 0.2 eV steps within the main edge, and coarse (2 to 5 eV) steps over the pre-edge and edge step regions. The U(VI) and U(IV) oxidation states were assigned half step height energies of 17,168.0 and 17,163.7 eV, using $UO_2(NO_3)_2$ and UO_2 (both diluted in SiO_2 powder), respectively (Figure 1c). Monochromator calibration at this high-energy region was done with Y foil, with its absorption edge taken as 17,038.0 eV.

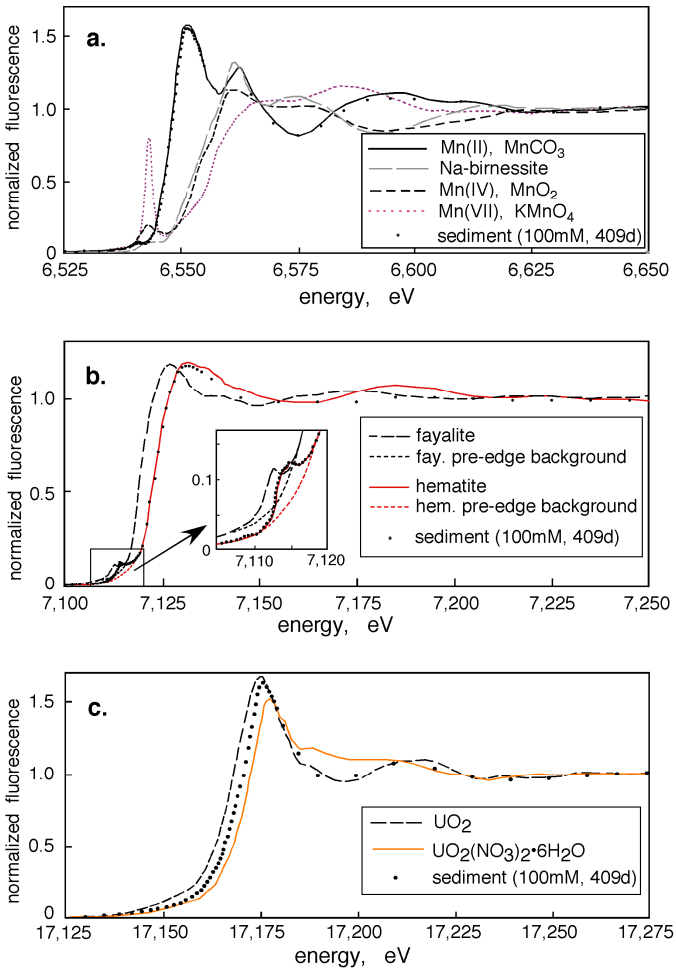

153

154 **Figure 1.** XANES spectra of oxidation state standards (**a.**) Mn K-edges, (**b.**) Fe K-edges with
155 insert close-up view of pre-edge peak region, and (**c.**) U L_{III} edges. Examples of spectra
156 collected from the 100 mM sediment column are also included.

157

158 **Results and Discussion**

159 While this paper is focused on changes in oxidation states of Mn, Fe, and U within sediments,
160 aspects of the effluent solution chemistry important for understanding redox transformations are
161 summarized in Figure 2 and Table S2. The main microbiological characteristics follow those
162 presented in our earlier study of U bioreduction (*14, 17*). Most of the lactate supplied to columns
163 was mineralized, such that bicarbonate levels in effluents were elevated in proportion to influent

OC concentrations (Figure 2a,b). Uranium concentrations rapidly decreased for columns supplied with OC ≥ 30 mM, followed by increased U concentrations resulting from formation of soluble U(VI) tricarbonate and dicalcium uranyl tricarbonate complexes (*14*), and reached steady values in the range of 0.5 to 30 µM after about 200 days (Figure 2c). The intermediate OC supply rate of 0.14 mmol kg^{-1} day^{-1} (10 mM OC influent) resulted in the highest effluent U concentrations because of enhanced U(VI) solubility from carbonate complexes while achieving only minor U reduction. The low levels of nitrate (50 µM) in influent solutions were reduced below detection (0.3 µM nitrate and nitrite) in effluents of all OC-supplied columns, and nearly completely reduced (2.4 ±2.4 µM in effluents) in the column that received no OC. Nitrate and nitrite have been shown to promote U(IV) reoxidation by directly serving as a TEA and through oxidizing Fe(II) to Fe(III), which in turn oxidizes U(IV) (*10, 15, 32*). Sulfate reduction was proportional to the OC supply, with total S levels in effluents falling below 5 µM in the 30 and 100 mM OC columns (Table S2).

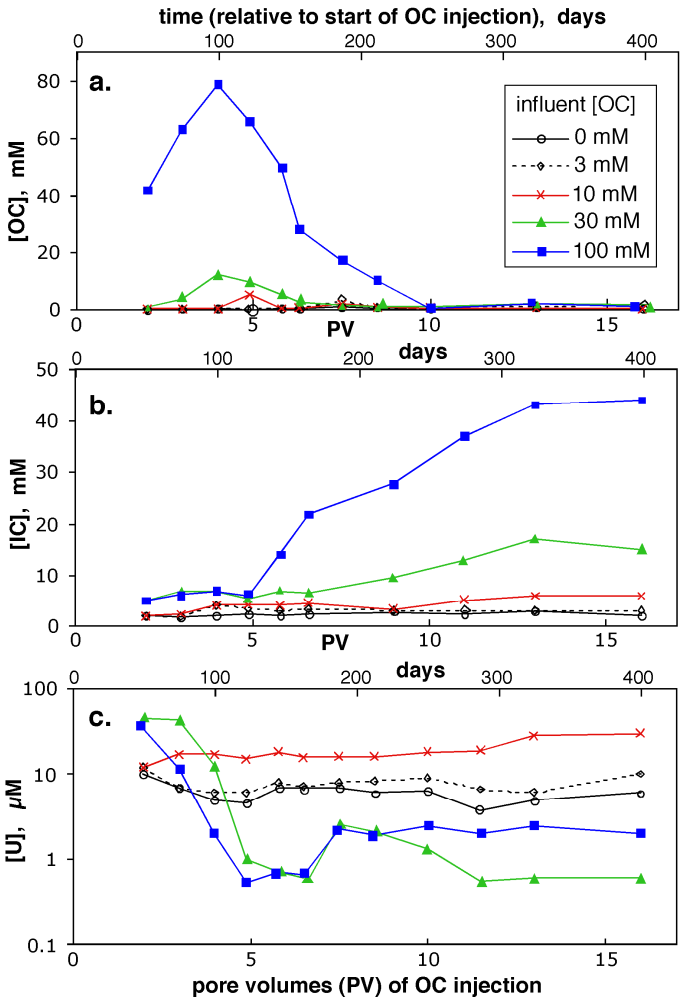

Figure 2. Trends in effluent concentrations for (**a.**) organic carbon (OC), (**b.**) inorganic carbon, and (**c.**) uranium in sediment columns supplied with different concentrations of OC.

Redox electrode measurements. Stable redox profiles developed by about 2.5 PV of OC solution infusion, with trends in Pt electrode data that reflected OC concentrations in influent solutions and distances along columns (Figure 3). Calculated Eh (*1*, *14*) for nitrate, Mn(IV), U(VI), Fe(III), and sulfate reduction are included in Figure 3 for comparison. Although the redox measurements are very local and have relatively large uncertainties (1), several conditions

are evident. Without addition of OC, redox potentials remained oxidizing, indicating that native sediment organic matter mineralization rates were low. The 30 and 100 mM OC columns have redox potentials that have fallen below levels for Mn reduction. The sediment supplied with 3 and 10 mM OC exhibited redox gradients, reflecting OC oxidation during transit.

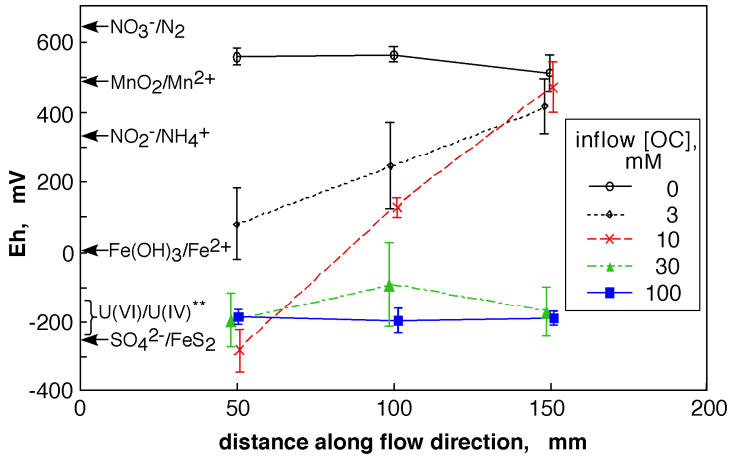

Figure 3. Redox potential profiles measured with Pt electrodes in columns. Data points are averages of measurements obtained at 2.5, 5.9, 7.3, 10.0, and 12.7 PV (days 70 to 330) relative to the start of OC infusion. Range bars indicate standard deviations. Also shown along the Eh axis are calculated potentials (all at pH 7.3) for nitrate reduction (NO_3^- = 1 µM, $P(N_2)$ = 0.8 atm), Mn(IV) reduction (pyrolusite, Mn^{2+} = 10 µM), nitrite reduction to ammonia (equimolar N species), Fe(III) reduction (ferrihydrite, Fe^{2+} = 1 µM), **U(VI) reduction ($Ca_2UO_2(CO_3)_3$ = 1 mM, U(IV) = UO_2(am), Eh ranges span pCO_2 = 2 to 1.5 and Ca^{2+} = 0.1 to 1.0 mM), and sulfate reduction to pyrite (1 µM Fe^{2+}, 0.1 mM SO_4^{2-}).

µ-XANES of Mn, Fe, and U. Time trends in column-averaged characteristic energies of Mn edges, Fe pre-edges, and U edges are shown in Figure 4, along with reference energies for oxidation state end members. Sediments with intermediate levels of OC influxes (especially the 3 and 10 mM OC columns) were measured on fewer occasions. The 0, 30, and 100 mM OC

treatments exhibited no significant spatial gradients in Mn, Fe, and U oxidation state profiles. In contrast, the sediment column receiving 10 mM OC solutions showed spatial gradients in oxidation states (Figure 5). Micro-XANES measurements on the 3 mM OC treated sediment were only obtained at end of this study (average energies shown in Figure 4), and yielded Mn, Fe, and U oxidation state profiles (not shown) similar to those of the 10 mM OC treatment.

Manganese oxidation state trends. Micro-XANES spectra obtained on the initial sediment showed that Mn occurred in intermediated oxidation states, with very little variability in the K-edge absorption energies (Figure 4a). Because Mn(III,IV) oxides suppress U bioreduction rates, and also oxidize uraninite (12), the initial redox status of Mn reflects geochemical conditions unfavorable for U reduction. Upon starting inflow, highly variable reduction occurred during the initial stage when only synthetic groundwater (no added OC) was being supplied, reflecting redox instability often observed upon rewetting sediments (*33*). This was followed by systematically OC-dependent trends during the remainder of the experiment (Figure 4a). The µ-XANES spectra obtained on sediments infused with 30 and 100 mM OC had Mn K-edge energies identical to those of Mn(II) standards (Figure 1a), showing rapid and complete conversion to Mn(II) by 2.1 PV. Although a relative uncertainty of about 5% is associated with oxidation states obtained from these Mn µ-XANES measurements, corresponding to ±2 mmol Mn kg^{-1}, rapid and monotonic reduction of Mn in the 30 and 100 mM OC treatments indicates that Mn(III,IV) oxides are no longer present, hence are not involved in U reoxidation. Even the sediment receiving 0 mM OC exhibited gradual Mn reduction, apparently from slow oxidation of native sediment organic matter. Sediments permeated with 3 and 10 mM OC exhibited intermediate rates of Mn reduction.

Spatial distributions of Mn K-edge energies along the 10 mM OC column at days 174, 266, and 409 are shown in Figure 5a. The presence of a thick wall section prevented collection of μ-XANES data in the vicinity of 100 mm. Note that Mn in the region closest to the OC supply was more reduced than regions further along the flow path, consistent with redox electrode data, and reflecting kinetically favorable reduction under OC-limited conditions. Also note that at the nominally 800 μm measurement scale of individual data points, local spatial variability in Mn oxidations is significant until reduction to Mn(II) is completely achieved.

Iron oxidation state trends. Based on Fe pre-edge peak centroid energies, initial sediment samples had a ratio of ferric to total Fe, Fe(III)/∑Fe, of 0.88 ±0.10. Even after 400 days (16 PV) of OC infusion, μ-XANES spectra indicated that the Fe(III)/∑Fe remained ≥ 0.76 ±0.10 (Figure 4b). Thus, in strong contrast to the rapid and complete reduction of Mn in sediments supplied with the higher levels of OC, overall Fe oxidation states remained relatively unchanged. It should be noted that although overall Fe oxidation states changed little, some of these changes were statistically highly significant. In particular, the Fe reduction/oxidation cycles that occurred from days 112 to 266 for the 30 and 100 mM OC sediments were significant at $p \leq 0.001$. The cause of these Fe redox fluctuations (measured average fluctuations amounted to 140 mmol kg^{-1}, with a standard deviation of 60 mmol kg^{-1}) was not identified, but possible coupling with U oxidation state changes is discussed later.

The reactive fraction of the sediment Fe is operationally defined, depending on reactions and time-scales of interest (*34*, *35*). For conditions imposed in this experiment, the citrate-dithionite extraction appears to provide a fair estimate of the reactive Fe fraction. The citrate-dithionite extraction removed 21% of this sediment's total Fe (Table S1), and the range of variation in Fe(III)/∑Fe determined by μ-XANES spectroscopy was of similar magnitude

(Figure 4b). The resistance to reduction of most of the sediment Fe(III), shown here through time trends in Fe K-edge μ-XANES spectra, is consistent with extraction-based characterizations of Fe in reducing sediments (*36*). Lack of detectable spatial trends in overall Fe oxidation state is shown in the μ-XANES profiles from the 10 mM OC column (Figure 5b). All other columns had similar, Fe(III)-dominated oxidation state profiles. Continued abundance of Fe(III) (> 800 mmol kg^{-1}) shows persistence of a high potential oxidizing capacity, with its impact strongly moderated by low Fe(III) reduction rates. It should also be noted that only a fraction of the total sediment Fe(III) consisting of poorly crystalline phases is capable of oxidizing U(IV) (*14, 16*).

Uranium oxidation state trends. Uranium L_{III} μ-XANES spectra on the original sediment showed that U occurred largely (93 ±7%) as U(VI). The control column supplied with the synthetic groundwater without OC exhibited only small variations from this initial state throughout the experiment (Figure 4c). Fluctuations in U L_{III} edge energies observed at early stages of the experiment apparently reflect transient redox changes occurring during establishment of water-saturated conditions. Micro-XANES measurements were obtained at fewer times for the sediments treated with 3 and 10 mM OC, but their results show levels of U reduction that are intermediate to those of the 0 versus 30 and 100 mM OC systems. Spatial profiles of U L_{III}-edge absorption energies measured in the 10 mM OC-treated sediment (Figure 5c) show U generally occurring in more reduced forms closer to the inlet, remaining more oxidized toward the outlet end, and retaining a high level of local oxidation state variability. The heterogeneous nature of local U oxidation states was confirmed through duplicate profile measurements of U L_{III}-edge energies on days 266 and 409 (data points with common x values in Figure 5c). Reproducibility of such duplicate scans demonstrated that X-ray beam induced redox

changes were insignificant for not only U, but for Mn and Fe (Figures 5a,b) as well, under our operating conditions.

Rapid U reduction followed by reoxidation was observed in the columns supplied with 30 and 100 mM influent OC concentrations (Figure 4c), similar to U redox changes reported in our previous study (14). The increases in U oxidation states measured on day 174 (relative to days 62 and 112) in the sediments supplied with 30 and 100 mM OC solutions were significant at $p \leq 0.001$. Uranium µ-XANES spectra obtain on day 266 showed further reduction, also significant at $p \leq 0.001$. The magnitude of U redox fluctuations measured in the 30 and 100 mM OC systems (days 62 to 266) both amounted to 28% of the full U(IV)/U(VI) edge shift, and are equivalent to transfers of 0.60 mmol e^- kg^{-1}. These measured U oxidation state reversals are complimentary in their directions to the Fe oxidation state variations measured over the same time interval. Net oxidation of U coincided with net reduction of Fe, and vice versa, qualitatively supportive of their redox coupling. Because of very similar potentials for U(VI)/U(IV) and Fe(III)/Fe(II) redox reactions, different Fe minerals have significantly different impacts on U speciation (*14, 16*). However, electron transfers of the magnitude measured for U oxidation state changes are below detection for Fe by µ-XANES spectroscopy because of the high total Fe in the sediment (1,185 mmol kg^{-1}), and the very large differences in concentrations of total Fe and U (Fe:U molar ratio = 1,100). Thus, the Fe µ-XANES spectroscopy is useful for identifying the persistence of Fe(III) and its potential availability as a TEA for U reoxidation, but Fe-U redox coupling could not be stoichiometrically quantified.

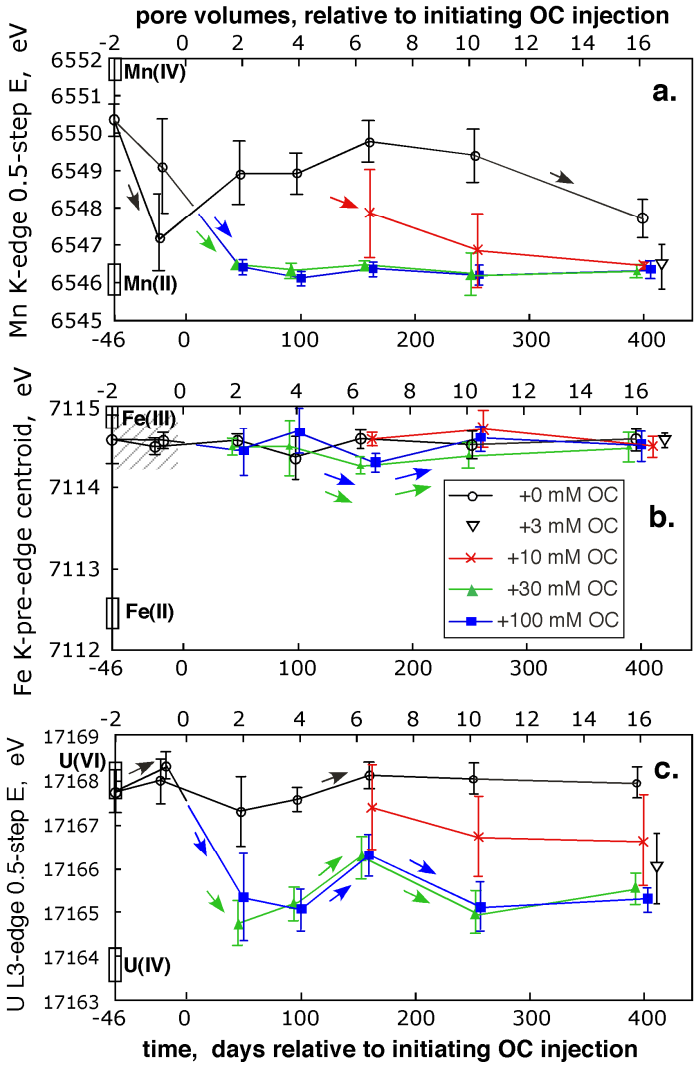

Figure 4. Time trends of column-average X-ray absorption energies for (**a.**) Mn K-edge, (**b.**) Fe K-edge pre-edge peak centroid, and (**c.**) U L_{III}-edge in sediment columns infused with different concentrations of OC. Data points are slightly shifted along the time axis for clarity. Energies of end member oxidation states are shown on the y-axes. Range bars indicate 1 standard deviation. The diagonally slashed band in the Fe graph indicates the range of energy shift possible if only the citrate-dithionite extractable Fe is completely reduced. Arrows indicate where energy differences between adjacent times (or relative to the initial sediment in cases where intermediate time measurements were unavailable) are significantly different at $p \leq 0.001$.

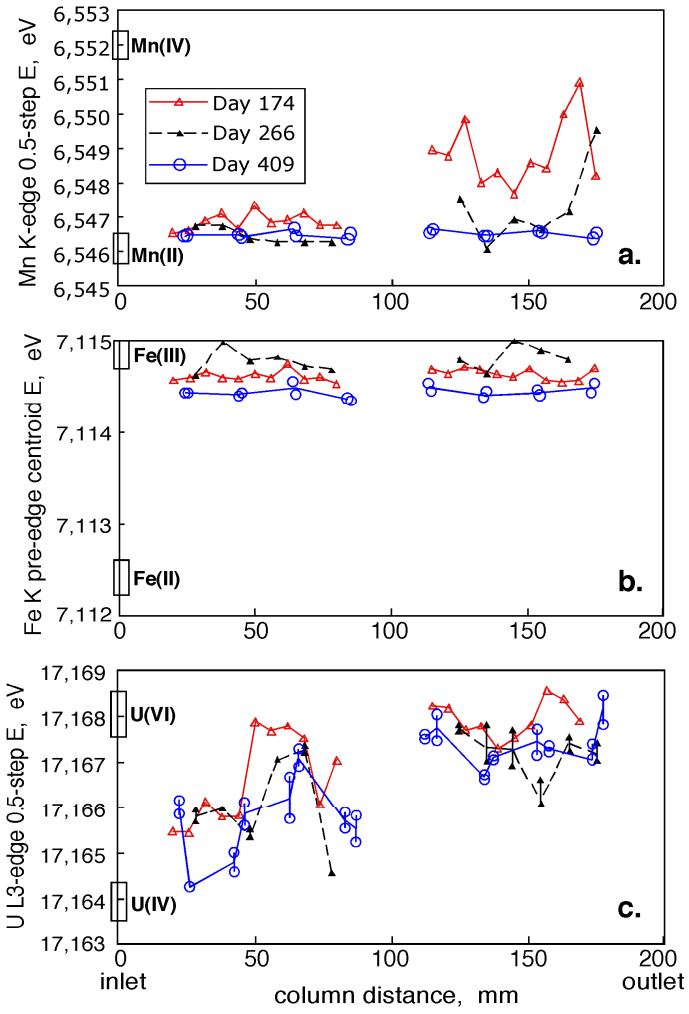

Figure 5. Profiles of characteristic X-ray absorption energies for (**a.**) Mn, (**b.**) Fe, and (**c.**) U, in the sediment supplied with 10 mM OC, obtained on days 174, 266, and 409 (relative to the start of OC injection). Duplicate scans were performed on U profiles obtained on both days 266 and 409, and shown in data points having common x (distance) values. Reference energies for end member oxidation states are indicated along the y-axes. A wall section prevented measurements in the center segment of the column.

Final measurements on day 409 suggest stability of the U redox status in sediments supplied with 30 and 100 mM OC, but with incomplete reduction. Even during this late phase of reduction, about 20% of the U remained as U(VI). Factors responsible for incomplete conversion to U(IV) could include oxidation by Fe(III), and irreversible sorption of some U(VI) on mineral surfaces (*37-39*).

Implications for OC-based, in-situ U reduction

The hypothesis that a reactive Fe(III) fraction served as the TEA for U reoxidation was supported through these in situ real-time µ-XANES measurements of Mn, Fe, and U. Most of the Fe(III) remained after complete reduction of Mn, and 80% U reduction. In contrast to Mn, the high mass fraction of Fe(III) in sediments with slow reduction allow Fe(III) phases to persist under reducing conditions over extended periods of time. Reduction of reactive, poorly crystalline Fe(III) (hydr)oxides appears necessary before stable U reduction is achievable. Finally, this work shows that although reoxidized U is later further reduced under a continuous supply of OC, a U(VI) fraction remained after over 400 days of reduction.

Acknowledgments

We thank Andrew Mei and Don Herman for technical assistance and the anonymous reviewers for helpful comments. Funding was provided through the Basic Energy Sciences, Geosciences Research Program, and the Environmental Remediation Sciences Program of the U. S. Department of Energy, under Contract No. DE-AC02-05CH11231. Portions of this work were performed at GeoSoilEnviroCARS (Sector 13), Advanced Photon Source (APS), Argonne National Laboratory. GeoSoilEnviroCARS is supported by the National Science Foundation -

Earth Sciences (EAR-0217473), Department of Energy - Geosciences (DE-FG02-94ER14466) and the State of Illinois. Use of the APS was supported by the U.S. Department of Energy, Office of Science, Office of Basic Energy Sciences, under Contract No. W-31-109-ENG-38. Portions of this work were performed at Beamline X26A, National Synchrotron Light Source (NSLS), Brookhaven National Laboratory. X26A is supported by the Department of Energy (DOE) - Geosciences (DE-FG02-92ER14244 to The University of Chicago - CARS) and DOE - Office of Biological and Environmental Research, Environmental Remediation Sciences Div. (DE-FC09-96-SR18546 to the University of Georgia). Use of the NSLS was supported by DOE under Contract No. DE-AC02-98CH10886.

Supporting Information Available

Elemental analyses of the initial sediment is provided in Table S1. Representative effluent chemical composition (U, Mn, Fe, and S) data are presented in Table S2. A diagram of the soil column is presented in Figure S1. This material is available free of charge via the Internet at http://pubs.acs.org.

Literature Cited

(1) Langmuir, D. *Aqueous Environmental Geochemistry*; Prentice-Hall: Upper Saddle River, NJ, 1997.

(2) Lovley, D. R.; Roden, E. E.; Phillips, E. J. P.; Woodward, J. C. Enzymatic iron and uranium reduction by sulfate-reducing bacteria. *Marine Geology* **1993**, *113*, 41-53.

(3) Anderson, R. T.; Vrionis, H. A.; Ortiz-Bernad, I.; Resch, C. T.; Long, P. E.; Dayvault, R.; Karp, K.; Marutzky, S.; Metzler, D. R.; Peacock, A.; White, D. C.; Lowe, M.; Lovley, D. R. Stimulating the in situ activity of Geobacter species to remove uranium from the groundwater of a uranium-contaminated aquifer. *Applied and Environmental Microbiology* **2003**, *69*, 5884-5891.

(4) Wall, J. D.; Krumholz, L. R. Uranium reduction. *Annual Review of Microbiology* **2006**, *60*, 149-166.

(5) Jeon, B. H.; Dempsey, B. A.; Burgos, W. D.; Barnett, M. O.; Roden, E. E. Chemical reduction of U(VI) by Fe(II) at solid-water interface using natural and synthetic Fe(III) oxides. . *Environmental Science and Technology* **2005**, *39*, 5642-5649.
(6) O'Loughlin, E. J.; Kelly, S. D.; Cook, R. E.; Csencsits, R.; Kemner, K. M. Reduction of uranium(VI) by mixed iron(II)/iron(III) hydroxide (green rust): Formation of UO2 nanoparticles. *Environmental Science and Technology* **2003**, *37*, 721-727.
(7) Beyenal, H.; Sani, R. K.; Peyton, B. M.; Dohnalkova, A. C.; Amonette, J. E.; Lewandowski, Z. Uranium immobilization by sulfate-reducing biofilms. *Environmental Science and Technology* **2004**, *38*, 2067-2074.
(8) Abdelouas, A.; Lutze, W.; Nuttall, H. E. Oxidative dissolution of uraninite precipitated on Navajo sandstone. *Journal of Contaminant Hydrology* **1999**, *36*, 353-375.
(9) Zhou, P.; Gu, B. Extraction of oxidized and reduced forms of uranium from contaminated soils: Effects of carbonate concentration and pH. *Environmental Science and Technology* **2005**, *39*, 4435-4440.
(10) Senko, J. M.; Istok, J. D.; Suflita, J. M.; Krumholz, L. R. In-situ evidence for uranium immobilization and remobilization. *Environmental Science and Technology* **2002**, *36*, 1491-1496.
(11) Istok, J. D.; Senko, J. M.; Krumholz, L. R.; Watson, D.; Bogle, M. A.; Peacock, A.; Chang, Y.-J.; White, D. C. In situ bioreduction of technitium and uranium in a nitrate-contaminated aquifer. *Environmental Science and Technology* **2004**, *38*, 468-475.
(12) Fredrickson, J. K.; Zachara, J. M.; Kennedy, D. W.; Liu, C.; Duff, M. C.; Hunter, D. B.; Dohnalkova, A. Influence of Mn oxides on the reduction of uranium (VI) by the metal-reducing bacterium Shewanella putrefaciens. . *Geochimica Cosmochimica Acta* **2002**, *66*, 3247-3262.
(13) Sani, R. K.; Peyton, B. M.; Dohnalkova, A.; Amonette, J. E. Reoxidation of reduced uranium with iron(III) (hydr)oxides under sulfate-reducing conditions. *Environmental Science and Technology* **2005**, *39*, 2059-2066.
(14) Wan, J.; Tokunaga, T. K.; Brodie, E. L.; Wang, Z.; Zheng, Z.; Herman, D. J.; Hazen, T. C.; Firestone, M. K.; Sutton, S. R. Reoxidation of bioreduced uranium under reducing conditions. *Environmental Science and Technology* **2005**, *39*, 6162-6169.
(15) Senko, J. M.; Mohamed, Y.; Dewers, T. A.; Krumholz, L. R. Role of Fe(III) minerals in nitrate-dependent microbial U(IV) oxidation. *Environmental Science and Technology* **2005**, *39*, 2529-2536.
(16) Ginder-Vogel, M.; Criddle, C. S.; Fendorf, S. Thermodynamic constraints on the oxidation of biogenic UO2 by Fe(III) (hydr)oxides. *Environmental Science and Technology* **2006**, *40*, 3544-3550.
(17) Brodie, E. L.; DeSantis, T. Z.; Joyner, D. C.; Baek, S. M.; Larsen, J. T.; Anderson, G. L.; Hazen, T. C.; Richardson, P. M.; Herman, D. J.; Tokunaga, T. K.; Wan, J. M.; Firestone, M. K. Application of a high-density oligonucleotide microarray approach to study bacterial population dynamics during uranium reduction and reoxidation. *Applied and Environmental Microbiology* **2006**, *72*, 6288-6298.
(18) Roden, E. E.; Zachara, J. M. Microbial reduction of crystalline iron(III) oxides: Influence of oxide surface area and potential for cell growth. *Environmental Science and Technology* **1996**, *30*, 1618-1628.
(19) Lovley, D. R.; Phillips, E. J. P. Rapid assay for microbially reducible ferric iron in aquatic sediments. *Applied and Environmental Microbiology* **1987**, *53*, 1536-1540.
(20) Zavarin, M. In *Soil Science*; University of California: Berkeley, 1999; Vol. Ph. D., p 279.

(21) Bertsch, P. M.; Hunter, D. B. Applications of synchrotron-based x-ray microprobes. *Chemical Reviews* **2001**, *101*, 1809-1842.
(22) Sutton, S. R.; Bertsch, P. M.; Newville, M.; Rivers, M.; Lanzirotti, A.; Eng, P. Microfluorescence and microtomography analyses of heterogeneous earth and environmental materials. In *Applications of Synchrotron Radiation in Low-Temperature Geochemistry and Environmental Science*; Fenter, P. A., Rivers, M. L., Sturchio, N. C., Sutton, S. R., Eds.; Mineralogical Society of America: Chantilly, VA, 2002; Vol. 49, pp 429-483.
(23) Ross, D. S.; Hales, H. C.; Shea-McCarthy, G. C.; Lanzirotti, A. Sensitivity of soil manganese oxides: XANES spectroscopy may cause reduction. *Soil Science Society of America Journal* **2001**, *65*, 744-752.
(24) Riggs-Gelasco, P. J.; Mei, R.; Ghanotakis, D. F.; Yocum, C. F.; Penner-Hahn, J. E. X-ray absorption spectroscopy of calcium-substituted derivatives of the oxygen-evolving complex of Photosystem II. *Journal of the American Chemical Society* **1996**, *118*, 2400-2410.
(25) Gorry, P. A. General least-squares smoothing and differentiation by the convolution (Savitzky-Golay) method. *Analytical Chemistry* **1990**, *62*, 570-573.
(26) Negra, C.; Ross, D. S.; Lanzirotti, A. Oxidation behavior of soil manganese: Interactions among abundance, oxidation state, and pH. *Soil Science Society of America Journal* **2005**, *69*, 87-95.
(27) Bajt, S.; Sutton, S. R.; Delaney, J. S. X-ray microprobe analysis of iron oxidation states in silicates and oxides using X-ray absorption near edge structure (XANES). *Geochimica Cosmochimica Acta* **1994**, *58*, 5209-5214.
(28) Wilke, M.; Farges, F.; Petit, P.-E.; Brown, G. E., Jr.; Martin, F. Oxidation state and coordination of Fe in minerals: An Fe K-XANES spectroscopic study. *American Mineralogist* **2001**, *86*, 716-730.
(29) Berry, A. J.; O'Neill, H. S. C.; Jayasuriya, K.; Campbell, S. J.; Foran, G. J. XANES calibrations for the oxidation state of iron in silicate glass. *American Mineralogist* **2003**, *88*, 967-977.
(30) La Force, M. J.; Fendorf, S. Solid-phase iron characterization during common selective sequential extractions. *Soil Science Society of America Journal* **2000**, *64*, 1608-1615.
(31) Duff, M. C.; Morris, D. E.; Hunter, D. B.; Bertsch, P. M. Spectroscopic characterization of uranium in evaporation basin sediments. *Geochimica Cosmochimica Acta* **2000**, *64*, 1535-1550.
(32) Finneran, K. T.; Housewright, M. E.; Lovley, D. R. Multiple influences of nitrate on uranium solubility during bioremediation of uranium-contaminated subsurface sediments. *Environmental Microbiology* **2002**, *4*, 510-516.
(33) Bartlett, R.; James, B. Studying dried, stored soil samples -some pitfalls. *Soil Science Society of America Journal* **1980**, *44*, 721-724.
(34) Roden, E. E. Analysis of long-term bacterial vs. chemical Fe(III) oxide reduction kinetics. *Geochimica Cosmochimica Acta* **2004**, *68*, 3205-3216.
(35) Hyacinthe, C.; Bonneville, S.; Van Cappellen, P. Reactive iron(III) in sediments: Chemical versus microbial extractions. *Geochimica Cosmochimica Acta* **2006**, *70*, 4166-4180.
(36) Lovley, D. R.; Phillips, E. J. P. Availability of ferric iron for microbial reduction in bottom sediments of the freshwater tidal Potomac River. *Applied and Environmental Microbiology* **1986**, *52*, 751-757.

(37) Jeon, B. H.; Kelly, S. D.; Kemner, K. M.; Barnett, M. O.; Burgos, W. D.; Dempsey, B. A.; Roden, E. E. Microbial reduction of U(VI) at the solid-water interface. *Environmental Science and Technology* **2004**, *38*, 5649-5655.
(38) Giammar, D. E.; Hering, J. G. Time scales for sorption-desorption and surface precipitation of uranyl on goethite. *Environmental Science and Technology* **2001**, *35*, 3332-3337.
(39) Ortiz-Bernad, I.; Anderson, R. T.; Vrionis, H. A.; Lovley, D. R. Resistance of solid-phase U(VI) to microbial reduction during in situ bioremediation of uranium-contaminated groundwater. *Environmental Microbiology* **2004**, *70*, 7558-7560.